Anatomical characterisation of three different psychosurgical targets in the subthalamic area: from the basal ganglia to the limbic system

Marie Neiges Santin, Nicolas Tempier, Hayat Belaid, Matthieu Zenoni, Sylvie Dumas, Åsa Wallén-Mackenzie, Eric Bardinet, Christophe Destrieux, Chantal François, Carine Karachi

Anatomical characterisation of three different psychosurgical targets in the subthalamic area: from the basal ganglia to the limbic system

Marie Neiges Santin
Sorbonne Université, Institut du Cerveau – Paris Brain Institute- ICM, CNRS, APHP, Hôpital de la Pitié Salpêtrière
Nicolas Tempier
Sorbonne Université, Institut du Cerveau – Paris Brain Institute- ICM, CNRS, APHP, Hôpital de la Pitié Salpêtrière
Hayat Belaid
Hôpital Fondation Adolphe de Rothschild
Matthieu Zenoni
Sorbonne Université, Institut du Cerveau – Paris Brain Institute- ICM, CNRS, APHP, Hôpital de la Pitié Salpêtrière
Sylvie Dumas
Oramacell
Åsa Wallén-Mackenzie
Uppsala University
Eric Bardinet
Sorbonne Université, Institut du Cerveau – Paris Brain Institute- ICM, CNRS, APHP, Hôpital de la Pitié Salpêtrière
Christophe Destrieux
UMR Inserm U1253, Université de Tours
Chantal François
Sorbonne Université, Institut du Cerveau – Paris Brain Institute- ICM, CNRS, APHP, Hôpital de la Pitié Salpêtrière
Carine KARACHI (carine.karachi@gmail.com)
Sorbonne Université, Institut du Cerveau – Paris Brain Institute- ICM, CNRS, APHP, Hôpital de la Pitié Salpêtrière

---

Research Article

Keywords: subthalamic nucleus, Sano triangle, medial forebrain bundle, immunohistochemistry, psychiatric disease, DBS

Posted Date: February 7th, 2023

DOI: https://doi.org/10.21203/rs.3.rs-2546607/v1

Version of Record: A version of this preprint was published at Brain Structure and Function on September 5th, 2023. See the published version at https://doi.org/10.1007/s00429-023-02691-2.

Abstract

Effective neural stimulation for the treatment of severe psychiatric disorders needs accurate characterisation of surgical targets. This is especially true for the medial subthalamic region (MSR) which contains three targets: the anteromedial STN for obsessive compulsive disorder (OCD), the medial forebrain bundle (MFB) for depression and OCD, and the “Sano triangle” for pathological aggressiveness. Blocks containing the subthalamic area were obtained from two human brains. After obtaining 11.7-Tesla MRI, blocks were cut in regular sections for immunohistochemistry. Fluorescent *in situ* hybridisation was performed on the macaque MSR. Electron microscopic observation for synaptic specialisation were performed on human and macaque subthalamic fresh samples. Images of human brain sections were reconstructed in a cryoblock which was registered on the MRI and histological slices were then registered. The STN contains glutamatergic and fewer GABAergic neurons and has no strict boundary with the adjacent MSR. The anteromedial STN has abundant dopaminergic and serotoninergic innervation with sparse dopaminergic neurons. The MFB is composed of dense anterior dopaminergic and posterior serotoninergic fibres, and fewer cholinergic and glutamatergic fibres. Medially, the Sano triangle contains orexinergic terminals from the hypothalamus, and neurons with strong nuclear oestrogen receptor-alpha staining with a decreased anteroposterior and mediolateral gradient of staining. These findings provide new insight regarding MSR cells and their fibre specialisation, forming a transition zone between the basal ganglia and the limbic systems. Our 3D reconstruction enabled us to visualise the main histological features of the three targets which should enable better targeting and understanding of neuromodulatory stimulation results in severe psychiatric conditions.

Introduction

Using neuromodulation of specific brain networks to treat psychiatric disorders is gaining interest, with both selective lesions and deep brain stimulation (DBS). Even though encouraging results have been obtained using neuromodulation of limbic brain networks, around half of patients remain poor responders or even treatment resistant without any clear explanations. From an anatomical point of view, therapeutic targets remain poorly defined and no surgical tool seems to be precise enough to reach the individually defined targets. This is especially true for the subthalamic area which comprises the subthalamic nucleus (STN) and its adjacent medial subthalamic region (MSR) which extends to the wall of the third ventricle. Three different surgical targets for psychosurgery have been proposed within the MSR,: the anteromedial STN, used to treat severe obsessive compulsive disorders (OCD) (Mallet et al. 2008; Chabardes et al. 2020), the medial forebrain bundle (MFB) to treat resistant depression (Schlaepfer et al. 2013; Coenen et al. 2019) and recently OCD (Coenen et al. 2016), and the so-called “Sano triangle” to treat pathological aggressiveness (Sano 1962; Sano et al. 1966, 1970, Torres et al. 2013, 2020; Micieli et al. 2017). These three regions are anatomically close to each other with no clear-cut boundaries, and their different neuronal and fibre types remain largely unknown in humans. This may explain the difficulty in interpreting psychiatric effects of neuromodulation in this area and to formulate physiological hypotheses regarding the effects obtained.

High frequency stimulation of the STN in some patients with Parkinson's disease (PD) has been reported to induce psychiatric symptoms such as hypomania (Welter et al. 2014), and to alleviate significantly OCD when stimulating the anteromedial part of the nucleus (Mallet et al. 2007). Following this finding in PD, an initial randomised double-blind trial was done in refractory OCD patients that demonstrated the ability for STN-DBS to significantly alleviate obsessions and compulsions. However, about a quarter of patients were unresponsive without obvious predictive factors (Mallet et al. 2008; Chabardes et al. 2020), whereas roughly half of the patients had a significant alleviation that surprisingly necessitated only a very small volume of activated tissue within the anteromedial STN. One possible explanation for these unpredictable results was that the optimal target is so small that DBS placement is very difficult to achieve, especially in the light of individual anatomical variability. Moreover, at present, no imaging tools could answer this question with high enough accuracy and especially if the goal is to reach neurons and pathways that could only be identified at the microscopic level.

Anatomically, the STN is not a homogeneous nucleus, with the highest density of its glutamatergic neurons being observed in its ventromedial part with a small population of GABAergic interneurons (Lévesque and Parent 2005). The STN receives two main projections from the cortex and from the external pallidum, with the anteromedial STN receiving mainly inputs from the limbic ventral pallidum (Karachi et al. 2005; Haynes and Haber 2013). The STN also receives multiple sources of innervation, with a sparse dopaminergic projection from the substantia nigra pars compacta and the ventral tegmental area as reported in monkeys (Lavoie et al. 1989; François et al. 2000) and humans (Augood et al. 2000), and an important serotoninergic and cholinergic innervation (Parent et al. 2011; Eid et al. 2014). Whether these different modulatory inputs homogeneously innervate the whole extent of the STN or are restricted to specific functional territories of the nucleus, is still to be determined and has important relevance for the understanding of the clinical effects observed following DBS, and would shed some light on the physiology basis of OCD.

Lying between the STN and the third ventricle, the MSR is poorly defined anatomically with numerous fibres of passage and sparse cell bodies (Temiz et al. 2019; Barbier et al. 2021). The MFB constitutes the biggest fibre bundle of the MSR, and contains both ascending and descending fibres of the mesolimbic pathways. These fibres are mainly dopaminergic and serotoninergic and lie along the dorsal border of the STN (Parent et al. 2011). The MFB, and especially its supero-lateral branch, is a relatively new target and its stimulation seems efficacious to alleviate depression (Schlaepfer et al. 2013; Coenen et al. 2016, 2019) and has shown interesting recent results in bipolar disorders (Gippert et al. 2017) and resistant OCD (Coenen et al. 2016; Oldani et al. 2021). The hypothetical mechanism of such therapy is that MFB high frequency stimulation activates basal forebrain structures and prefrontal cortex and may explain the clinical benefit obtained. Whether DBS of the MFB also modulates other neurotransmitters such as descending glutamatergic projections from the PFC remains to be determined (Schlaepfer et al. 2013).

In the most medial part of the MSR, the Sano triangle has been used as a target to treat pathological aggressiveness in schizophrenic and autism-spectrum disorders patients with stereotactic lesions in the 70's (Sano 1962; Sano et al. 1966, 1970), and more recently with DBS (Torres et al. 2013, 2020; Micieli et

al. 2017; Yan et al. 2022). The target first defined by Sano was within the posterior hypothalamus (Sano 1962; Sano et al. 1966, 1970). However, anatomically the Sano triangle is located posterior to the mammillary body which is actually defined as the posterior limit of the hypothalamus (Swaab 2003; Schaltenbrand et al. 2005; Nieuwenhuys et al. 2008). Due to this discrepancy and to the lack of clear boundaries, defining the Sano triangle is challenging. Its morphological organisation is not well-known in primates but roughly located between surrounding structures such as the posterior hypothalamus and the midbrain Periaqueductal Grey (Nauta et al. 1969; Carpenter 1991).

All these data highlight the fact that improved targeting for treatment-resistant psychiatric disorders needs a precise characterisation of the morphological organisation of targets within the subthalamic area in the primate brain. In this study, we aim to identify the main neuronal and fibre types present in the primate MSR. By using immunohistochemistry and fluorescent *in situ* hybridisation (FISH) in regularly spaced sections, we provide 2D and 3D maps of labelled fibres and cell bodies to allow precise delineation of the three targets: the anteromedial STN, the MFB and the Sano triangle. Our final aim is to be able to identify the neuronal populations, the axon terminals and the fibre bundles included in lesions or volume of activated tissue (VTA) induced by DBS in order to better understand the physiology basis of the effects of neuromodulation in these severe and resistant psychiatric diseases in a given patient.

Methods

Human brain samples

Four human brains were used for this study. Brain samples came from subjects who previously consented for organ donation: two were acquired from the Anatomy Department of University Paris 5–Descartes School of Medicine, and two from Anatomy Department of University of Tours School of Medicine. The brain samples were obtained following the guidelines approved by The National Consultative Ethics Committee for Health and Life Sciences, according to current French law for organ donation. The neurosurgeon performing the extraction (CK, CD) examined the whole brain macroscopically to check that no obvious lesions, including tumours, traumatic or vascular lesions. We also verified that the substantia nigra was well pigmented for the four specimens. For immunohistochemical characterisation, 2 brains (H1h and H2h) were carotid perfused with 4% paraformaldehyde (PFA) in phosphate buffer (PB). After extraction, blocks containing the whole extent of the STN, MSR and Sano triangle on both sides were fixed by immersion in 4% PFA for 8 days (H1h) and 11 days (H2h) at 4°C. The H2H block was scanned using a 11.7-Tesla scanner (Biospec 117/16, Bruker Biospin) equipped with a 72 mm transceiver. A 1:200 gadolinium MR contrast agent was added to the PB 48 hours prior to imaging. A T2*-weighted image was acquired with FOV 5.63*6.33*6.68 cm^3; matrix size 512*576*608 leading to an isotropic resolution of 110 µm, with a TE/TR = 7.5/17 ms, using 12 signal averages for a total of 6h 57min acquisition time.

After the MRI acquisition, the block was frozen at -80°C in dry ice and cut in 151 slices with a width of 50 µm. Each slice was photographed during sectioning, using a camera fixed on top of the microtome.

Fiducial markers on the freezing microtome were held constant across all images. A 3D reconstruction was made loading all the images to 3D Slicer and included a visual quality check and correction when needed as previously described (Yelnik et al 2007). The cryoblock was cropped and the intensity differences between slices was reduced using MATLAB image histogram matching algorithm. The cryoblock voxel spacings were measured based on the slice holder and the T2* structure size equivalents.

The blocks were then rinsed in phosphate-buffered saline (PBS) 0.1M and cryoprotected in 10, 20 then 30% sucrose in PB 0.1M. 50 µm coronal sections of the blocks were cut on a freezing microtome. For electron microscopic analyses, 2 other human brains (H3 and H4) were removed from the skull and each hemisphere cut into blocks containing the entire extent of the STN (cube with 18 mm sides). Blocks were immediately post-fixed by immersion in 4% PFA in 0.1M PBS for 72h at 4°C and then rinsed in 0.1M PBS. Tissue blocks were cut into 40 µm coronal sections using a vibratome (Microm HM 650 U) and collected in PBS 0.1M.

Macaque brain samples

We used 4 adult macaque brains, 3 *Macaca mulatta* and 1 *Macaca fascicularis*. Animal care was carried out in strict accordance with the European Union Directive of 2010 (Council Directive 2010/63/EU) for care and use of laboratory animals. The authorisation for conducting our experiments was approved by the Ethics Committee in Animal Experiment Charles Darwin (agreement no. Ce5/2011/014). The protocol was designed to minimize the number of animals and reduce their suffering and distress. The animals were tranquilised with ketamine 500 (10 mg/kg), received morphine (dolorex, 0.04 mg/kg) and were then deeply anesthetized with isoflurane (3%) and oxygen (50%). For immunohistochemical and electron microscopic analyses, 2 macaques (M1 and M2) were intracardially perfused with 4% PFA in PB. Similar to human brains, small blocks containing the entire extent of the STN (cube with 18 mm sides) were cut, post-fixed by immersion in PFA, rinsed and cut on a vibratome into 40 µm coronal sections. For *in situ* fluorescence hybridisation (FISH), the brains of 2 other macaques (M3 and M4) were removed from the skull and cut on a cryostat at 16 µm. Sections were mounted on slides and stored at -80°C.

Immunohistochemistry

Adjacent series of regularly spaced sections (1/10, 500 µm) of human and monkey brains were immunohistochemically processed for tyrosine hydroxylase (TH), orexin A (OX), anti-serotonin transporter (SERT), vesicular glutamate transporter 1 (VGluT1), choline acetyl transferase (ChAT), and oestrogen receptors of α type (ERα) and were incubated with secondary antibodies from the appropriate species (see Supplementary method 1 for details). Some sections were counterstained with cresyl violet. All sections were digitised using a Hamamatsu Nano Zoomer (Hamamatsu Photonics, France).

The subthalamic area was delineated by the subthalamic nucleus laterally, the zona incerta dorsally, the ventral tegmental area ventrally, the posterior hypothalamus anteriorly, and the wall of the third ventricle medially. Within the subthalamic area, the MFB was delineated using TH and SERT immunostained fibres and the Sano triangle using adjacent structures such as the mammillothalamic tract laterally and the

third ventricle medially, the zona incerta dorsally and the ventral tegmental area ventrally, the mammillary body anteriorly and the red nucleus posteriorly (Supplementary Fig. 1).

Quantification of dopaminergic and serotoninergic terminals in the STN

In order to confirm that TH innervation is dopaminergic and not noradrenergic, two coronal sections taken at mid levels of the STN in two brains were processed for TH and dopamine transporter (DAT) (Eid and Parent 2015) (supplementary method 2).

Sections were examined and imaged with a Leica DM4000B fluorescent microscope (Leica Microsystems, Nanterre, France). Quantification of TH-positive (TH+) and SERT + terminals in the STN was performed on two human and two monkey brains using a semi-automatic image analysis system. In order to quantify the distribution of thin, varicose labelled terminals and to correct for variations in the alignments of sections, the STN was subdivided into six subparts (Fig. 1A), drawn inside the three functional sensorimotor, associative and limbic territories of the STN provided by external pallidal projections (Fig. 1B). We quantified the number of labelled terminals which are within three squares of 50 µm side spaced by 100 µm randomly distributed by the computer within the 6 STN subparts. We counted all labelled terminals that were fully inside the squares or that crossed borders of the squares. The number of squares randomly selected in each STN sector was previously determined to ensure that the addition of another square would lead to a < 5% variation in the mean number of terminals per square. The density of finely labelled terminals was expressed as the number of labelled axons per mm^3 and was compared across the different subparts of the STN using a Kruskal-Wallis one-way ANOVA followed by Dunn's post-hoc test. The density of TH + and SERT + terminals was expressed as the number of labelled axons per mm^3.

Fluorescence in situ hybridisation (FISH)

To label with certainty glutamatergic and GABAergic cell bodies, we used FISH in fresh macaque brains. FISH was performed using antisense RNA probes directed towards the mRNA of the VGluT2 (NM_020346.3 sequence 1592–2014) and Gad1 (NM_000817.3: sequence 168–1064) genes (see detailed protocol in Dumas and Wallén-Mackenzie 2019, and Fortin-Houde et al 2022). Briefly, 16µm sections were hybridised in formamide hybridisation buffer containing probes labelled with fluorescein for the detection of mRNA. Fluorescein epitopes were then detected with horseradish peroxidase (HRP) conjugated anti-fluorescein antibody and revealed using Cy2-tyramide. DIG epitopes were detected with HRP anti-DIG Fab fragments and revealed using Cy3 tyramide. DAPI was used for nuclear staining. All slides were scanned at 20x magnification on a NanoZoomer 2.0-HT. Ndp2.view software (Hamamatsu) was used to view the images.

Electron Microscopy

After immunohistochemical development of TH or ChAT using diaminobenzidine with no addition of Triton X-100 to solutions, adjacent spaced sections were post-fixed in 1% (w/v) osmium tetroxide, incubated in 1% uranyl acetate, dehydrated and embedded in Epon 812. Ultrathin sections (70 nm thick) were cut, contrasted with uranyl acetate and lead citrate, and analysed on a JEOL (Akishima, Japan) 1200EX II electron microscope.

2D map and 3D visualisation

The T2* MRI was chosen as a reference 3D space to which all the data were registered (the cryoblock, the morphological and diffusion images and the immunostained histological slices). The cryoblock was registered to the T2* using a block-matching algorithm (Ourselin et al. 2000) using first a rigid and then a non-rigid method. The histological slices were first registered to their corresponding cryoblock slices using the block-matching algorithm with a rigid transform. After a 3D reconstruction of the histological slices using 3D slicer (Yelnik et al. 2007), the resulting 3D bloc was cropped in order to reduce its size while covering all the regions of interest. The 3D histological image was then deconstructed into slices. Each slice was registered to its corresponding cryoblock slice using the Landmark-based 2D thin-plate spline image registration algorithm to account for deformation generated by the immunohistochemistry process (temperature and cutting) (Sébille et al. 2019). The resulting images were 3D reconstructed to overlay with the cryoblock.

Results

Organisation of labelled MSR cell types

We found that the great majority of STN neurons expressed VGluT2 mRNA with a posterolateral to anteromedial density gradient, the anteromedial STN being the densest. We also found a small population of neurons expressing Gad mRNA homogeneously distributed within the STN (Fig. 2A).

Numerous neurons expressing VGluT2 mRNA were observed over the whole extent of the MSR, sometimes even within the MFB (Fig. 2B). The same observation was made for neurons expressing Gad mRNA, which were less numerous than the VGluT2 mRNA neurons. The density of these two types of neurons was lower in the Sano triangle than in the rest of the MSR, especially for neurons expressing Gad mRNA.

We detected a few TH + cell bodies in the anteromedial STN, close to the SN pars compacta (Fig. 3A) and in the anterior part of the Sano triangle (Fig. 3B) which correspond to the dopaminergic group A11, and none in the MSR.

As expected, OX + cell bodies were predominantly found anteriorly within the perifornical area of the hypothalamus (Fig. 3C). These OX + cell bodies extend posteriorly along the most antero-dorsal border of the STN and within the anterior part of the MFB (Fig. 3D).

We found numerous cell bodies with strong nuclear Erα staining within the whole MSR in continuity with the cell body staining in the hypothalamus and thalamus. There was a clear mediolateral and anteroposterior decreasing intensity gradient of staining in the MSR leading to dense stain anteromedially within the Sano triangle (Fig. 3E). Some neurons with low nuclear Erα staining extended up to the medial STN.

Organisation of labelled MSR axon terminals

At low magnification, VGluT1 staining appeared much weaker in the MSR than in other surrounding structures such as the thalamus or the striatum (Fig. 4A). At higher magnification, the staining appeared punctiform (Fig. 4A). VGluT1 + terminals were distributed over the whole extent of the MSR and were slightly more numerous in the Sano triangle.

Numerous thin, varicose, meandering TH + axons of passage and branching terminals coursed throughout the STN following a density gradient, with densely packed thin arborising varicose terminals in the anteromedial STN, and much sparser terminals in its ventral part (Fig. 4B). TH + terminal quantification was highest in the anteromedial part (n°1) ($p < 0.001$ when compared with other subparts), and then in the two dorsal subparts of the STN (n° 2d/3d) ($p < 0.001$ when compared with n° 2v/3v), in the posterolateral subpart (n° 4) ($p < 0.001$ when compared with n° 3v), and the ventral subparts of the central and dorsal STN (n° 2v/3v) (Table 1; Fig. 4A). This quantification follows a decreasing mediolateral and dorsoventral gradient of TH + terminal density. Under the electron microscope, numerous TH + axons contained electron-dense DAB reaction product that was occasionally very dense (Fig. 5). Many of these TH + axons were myelinated, especially in humans, observed both within the dorsal bundle to the STN as well as within the anteromedial and dorsal parts of the nucleus (Fig. 5A, B). TH + varicosities often established non-synaptic contacts in the STN. Symmetric synapses were also frequently observed in the anteromedial and dorsal subparts of the STN (Fig. 5C), while less numerous asymmetric synapses were also seen (Fig. 5D). Few TH + terminals was also detected in the whole MSR, with the Sano triangle being poorly innervated (Fig. 4B).

Compared to TH + innervation, the regional distribution of ChAT immunostaining was homogenous in the STN. Under the electron microscope, numerous unmyelinated ChAT + axons were observed (Fig. 5E, F). Numerous ChAT + varicosities containing small and clear vesicles and frequently mitochondria were observed in apposition to cell bodies and dendrites throughout the STN, whereas only a minority of ChAT + terminal varicosities were engaged in synaptic contacts mainly with unlabelled dendrites (Fig. 5G, H) and occasionally cell bodies, and were of the asymmetrical and more rarely of symmetrical type.

SERT + terminals ascended from the brainstem and arborised within the STN (Fig. 4C). The number of SERT + axons of passage and branching terminals were quantified in the STN subparts. The highest density of labelled axons was found in the anteromedial subpart (n° 1) ($p < 0.001$ when compared with n° 3d/3v), and then in the two central STN subparts (n° 2d/2v), in the postero-lateral subpart (n° 4), and in the two lateral STN subparts (n° 3d/3v) (Table 1). This indicates a decreased mediolateral gradient of

SERT + terminal density in the STN. SERT + fibres and varicose terminals were densely distributed in the MSR and especially within the Sano triangle (Fig. 4C).

Rare OX + varicose terminals were found homogeneously in the whole STN (Fig. 4D), and even more numerous in the Sano triangle but rare in the other part of the MSR (Fig. 4D).

Organisation of MFB labelled axons

A massive TH + bundle ascended anteriorly from the ventral tegmental area and the substantia nigra pars compacta (SNc), coursed along the dorsal STN border and constitutes the dopaminergic bundle of the MFB (Fig. 6). SERT + fibres, originating posteriorly in the dorsal raphe nucleus, coursed postero-anteriorly, passed partly through the ventral tegmental area and dorsomedially to the SNc, and ascended within the MFB dorsomedially to the STN (Fig. 6). This SERT + bundle was denser more posteriorly and extended more dorsolaterally than the TH + bundle. ChAT + fibres run along the dorsal border of the STN on their way to the thalamus and are thus part of the MFB. We also observed that VGluT1 + fibres were homogeneously distributed within the MFB without forming any fibre bundles.

Tridimensional visualisation of the STN, MFB and Sano triangle in the Human brain

The three surgical targets located in the subthalamic area are difficult to draw because of the lack of closed boundaries. Their delineations are based, at least partly, on adjacent brain structures. Even the medial limit of the anteromedial STN is impossible to draw with accuracy whatever the immunohistochemical staining. Here we delineated the three different targets in 2D based on the main morphological and histological features in order to visualise these main features in 3D. In general, we found that the anteromedial STN is characterised by a dense dopaminergic and serotoninergic innervation. The MFB is mainly constituted by compact dopaminergic and serotoninergic fibres. The Sano triangle showed numerous OX + fibres and numerous neurons expressing Erα with a mediolateral and anteroposterior decreasing density of staining (Fig. 7).

Table 1 : Number of TH+ and ChAT+ terminals per mm3 in the STN per individuals

	STN subparts					
Individual	n° 1 (x 10^3)	n° 2d (x 10^3)	n° 3d (x 10^3)	n° 4 (x 10^3)	n° 2v (x 10^3)	n° 3v (x 10^3)
TH M1	434 ± 75	285 ± 68	285 ± 37	194 ± 39	135 ± 44	121 ± 16
TH M2	385 ± 61	296 ± 58	282 ± 31	168 ± 64	124 ± 34	106 ± 18
TH H1	270 ± 26	174 ± 48	117 ± 27	87 ± 33	50 ± 26	41 ± 15
TH H2	275 ± 38	147 ± 58	85 ± 32	85 ± 28	61 ± 22	56 ± 14
ChAT M1	953 ± 84	942 ± 109	909 ± 91	974 ± 90	932 ± 88	1056 ± 139
ChAT M2	954 ± 61	957 ± 87	902 ± 121	992 ± 77	928 ± 71	994 ± 145
ChAT H1	752 ± 172	694 ± 163	694 ± 105	780 ± 178	786 ± 93	710 ± 70
ChAT H2	701 ± 61	741 ± 64	699 ± 88	747 ± 148	789 ± 40	789 ± 95

Data are presented as mean ± SD. M1, macaque n°1; M2, macaque n°2; H1, human n°1; H2, human n°2.

Discussion

Our study provides the first detailed description of the neural diversity of the anteromedial STN, the MFB and the Sano triangle using immunohistochemistry and FISH in the primate brain. The entire MSR that extends from the STN to the midline contains a majority of glutamatergic and GABAergic neurons and receives glutamatergic cortical terminals. The Sano triangle is characterised by the presence of numerous ERα receptors neurons and orexinergic terminals. The MFB is predominantly composed of dopaminergic, serotoninergic and cholinergic fibres organised in compact bundles, containing cholinergic and cortical glutamate fibres. The most striking characteristic of the anteromedial STN is its important dopaminergic and serotoninergic innervation compared to the other STN subparts. Moreover, its anteromedial part has no strict anatomical boundary with the adjacent MSR. These findings provide new insights regarding the morphological organisation and the cell and fibre specialisation of these three important targets for psychosurgery, highlighting the MSR as a transition zone between the basal ganglia and the limbic systems.

The anteromedial STN

The anteromedial STN appears to have a particular morphological organisation within the nucleus, with its medial border impossible to delineate from the MSR with the staining used. It has also already been shown that the dendrites of the STN neurons cross this anteromedial border in rats (Hammond and Yelnik 1983). It thus appears that the STN shares an indistinct border with the MSR, with possible shared axons terminals coming from the limbic GPe (Karachi et al. 2005). Moreover, tract tracing in monkeys and diffusion weighted imaging (DWI) in humans showed that limbic cortical axons project to the

anteromedial STN, straddling its border and extending densely to the MSR (Haynes and Haber 2013; Temiz et al. 2019). Our results confirm that the anteromedial STN has specific morphological characteristics that are different from the other parts of the STN. We confirmed that globally the STN has a low density of TH-positive terminals (Augood et al. 2000; Francois et al. 2000) and low concentrations of dopamine (Pifl et al. 1990). However, we observed a heterogeneous and graduated dopaminergic innervation, with a high density of terminals and cell bodies anteromedially. Moreover, ultrastructural observation showed the presence of TH + axon varicosities without synaptic specialisations mainly located in this anteromedial subpart, which suggests the existence of a volumic transmission of dopamine from the anteromedial to the other STN subparts (Fuxe et al. 1988). The STN serotoninergic innervation is also heterogeneous (Mori et al. 1985; Parent et al. 2010) and follows a decreasing mediolateral gradient similar to that of dopaminergic innervation. Conversely, cholinergic innervation is homogeneous throughout the nucleus. We found that GABAergic neurons, which are considered as interneurons, were distributed homogeneously throughout the whole STN, whereas they have been reported to be significantly more numerous in the anteromedial part in humans (Hardman et al. 2002; Levesque and Parent 2005). The fact that we did not find this distribution could be explained by the fact that we only mapped (and did not quantify) these neurons in monkeys and not at all in humans. Nevertheless, our data showed that the anteromedial STN is different from the other nucleus subparts, and suggest that dopamine and serotonin could play a specific role in emotional and motivational processing within the STN.

In the context of DBS in PD patients, the psychiatric adverse effects that may occur are commonly attributed to misplacing electrodes too anterior and ventromedial within the STN or to selecting ventral stimulating contacts (Somma et al. 2022). Moreover, recent electrophysiological experiments performed in PD and OCD patients that underwent STN-DBS confirmed that STN activity varies according to the location of the recording contacts within the nucleus, with a strong emotion-related and a weak motor-related modulation of oscillatory activity in the anterior-ventromedial compared to the posterior-dorsolateral STN subparts (Buot et al. 2013; Eitan et al. 2013). Interestingly, the magnitude of the emotional effect recorded varies according to the valence of the stimulus, with pleasant stimuli only encoded by OCD patients, without dopaminergic depletion, that were implanted into the anteromedial STN (Buot et al. 2021). Here, we suggest that the anteromedial limbic STN has the dual advantage of belonging to the basal ganglia and sharing its medial boundary with the MSR where limbic pathways such as the MFB are located. These anatomical features make the anteromedial STN an ideal theoretical DBS target to alleviate OCD, a disorder that involves dysfunction of the habit-formation and emotional networks.

The MFB

The MFB passes through the posterior MSR, located between the STN and the substantia nigra, the red nucleus, and the mammillo-thalamic tract (Coenen et al. 2019). The MFB comprises a large dopaminergic bundle originating in both the SNc and the ventral tegmental area. This dopaminergic branch of the MFB runs along the dorsal border of the STN on its way to the striatum (Lavoie et al. 1989). Interestingly, we

showed, within the dorsal border of the human STN, the presence of dopaminergic myelinated axons, a characteristic that has only previously been described in the basal ganglia of primates (Kung et al. 1998; Eid and Parent 2015). The MFB is a recent target for DBS to treat patients suffering first from treatment-resistant depression (Coenen et al. 2011, 2012, 2019; Fenoy et al. 2016) and second from severe OCD (Coenen et al. 2016). The action of high frequency stimulation of the MFB may activate these dopaminergic axons, and in particular those arising from the VTA and terminating within the nucleus accumbens (Miguel Telega et al. 2022). It is possible that the activation of this structure from its dopaminergic fibres could mediate both alleviation of mood and anti OCD effects. However, our results show that the MFB is also formed by a broad serotoninergic bundle following a roughly similar pathway (Parent et al. 2011), as well as by cholinergic (Eid et al. 2014) and glutamatergic fibres. This anatomical complexity makes the physiological hypothesis very wide and with poor specificity. Stimulating the MFB must thus probably activate all these different types of fibres. Moreover, it is probable that other fibres such as cortico-brainstem fibres or other microfibres and cell bodies present in the field of stimulation may also be recruited by the MFB-DBS (Haber et al. 2020). Their specific role regarding clinical results is still debated and difficult to determine.

The Sano triangle

We observed the presence of numerous neurons with a strong nuclear ERα labelling over the whole extent of the MSR, and especially in the medial and anterior part of the Sano triangle, an entity that was first described as a target to treat pathological aggressiveness. In the literature, high levels of ERα expression have been reported in the hypothalamus, and in other limbic brain areas such as the amygdala, the basal forebrain and the mammillary body (Osterlund et al. 2000; Kruijver et al. 2002; Perez et al. 2004). This suggests that the Sano triangle can be considered as a limbic structure *per se*. Previous experimental studies have shown the role of ERα hypothalamic neurons in aggressive behaviour, the lack of ERα gene severely reducing the production of aggressive behaviour in male mice (Ogawa et al 1997). The use of optogenetic techniques within the ventrolateral subdivision of the ventromedial hypothalamus (VMHvl) of mice has shown that activation of ERα + neurons could generate immediately aggressiveness. Interestingly, weaker optogenetic activation of these specific neurons promote sexual behaviour (Lee et al. 2014).

Another characteristic of the Sano triangle is its orexinergic innervation which is denser relative to other parts of the MSR. Orexin being a hypothalamic neuropeptide, this demonstrates direct projection from the hypothalamus to the Sano triangle. It is interesting to note that Orexin is reported as playing a role in regulating complex emotional responses (Soya and Sakura 2020), in particular in pathological anxiety and stress responses (Suzuki et al. 2005; Johnson et al. 2010). Another reason for considering the Sano triangle as limbic is the fact that it receives dense limbic cortical inputs (Temiz et al 2019), assessed here by the presence of VGluT1 terminals. Finally, the Sano triangle also contains a small dopaminergic neuronal population, which corresponds to the A11 group (Kitahama et al. 1998). These neurons, which project to the spinal cord (Barraud et al. 2010) are thought to be involved in painful conditions such as restless leg syndrome (Clemens et al. 2006) and particular headaches (Charbit et al. 2009). However, how

neuromodulation of which specific pathways within the Sano triangle could reduce pathological aggressive behaviour has still to be elucidated.

3D histological and deformable atlas for individual targeting

These three surgical targets within the MSR are particularly small and difficult to reach for a given patient. Improving targeting accuracy necessitates the development of high-quality imagery tools to take into account anatomical delineation using histological findings and diffusion sequences. The present study provided new insights into the 3D morphological organisation of cell and fibre components that are involved in the volume of activated tissue induced by DBS or in surgical lesions. In the near future, it would be useful to register this 3D atlas of the MSR to the individual MRI of patient in order to accurately localise the structure or substructure that we wish to target and stimulate. We believe that detailed morphological observations in 3D, together with individual diffusion MRI tractography and high-resolution morphological images, could improve the results of neuromodulation to alleviate severe and resistant psychiatric condition in the future.

Declarations

Statements and Declarations

Funding: Histological analyses were supported by a grant from the Fondation de France. MS is supported by Boston Scientific. NT is supported by through a grant from the ERIE foundation (TELOS). The non-human primate brains acquired through support from an ATIP-Avenir (INSERM) grant to Brian Lau.

Competing Interests: CK received fees from Boston scientific.

Author Contributions: We confirm that the manuscript has been read and approved by all named authors

Acknowledgement: We are grateful to Marie-Paule Muriel for her help and expertise for the electron microscopy. We are grateful to the anatomy department of “le Fer à Moulin” for providing human brain samples. We thank Max Westby for English editing.

References

1. Augood J, Hollingsworth ZR, Standaert DG, Emson C, Penney JB (2000) Localization of dopaminergic markers in the human subthalamic nucleus. J Comp Neurol 421(2):247–255.
2. Barbier M, Risold PY (2021) Understanding the Significance of the Hypothalamic Nature of the Subthalamic Nucleus. eNeuro 4;8(5):ENEURO.0116-21.2021. doi: 10.1523/ENEURO.0116-21.2021.
3. Barraud Q, Obeid I, Aubert I et al (2010) Neuroanatomical study of the A11 diencephalospinal pathway in the non-human primate. PLoS One 5(10):e13306. doi: 10.1371/journal.pone.0013306.
4. Blurton-Jones MM, Roberts JA, Tuszynski MH (1999) Estrogen receptor immunoreactivity in the adult primate brain: neuronal distribution and association with p75, trkA, and choline acetyltransferase. J

Comp Neurol 405(4):529–542.

5. Buot A, Karachi C, Lau B et al (2021) Emotions Modulate Subthalamic Nucleus Activity: New Evidence in Obsessive-Compulsive Disorder and Parkinson's Disease Patients. Biol Psychiatry Cogn Neurosci Neuroimaging 6(5):556–567.
6. Buot A, Welter ML, Karachi C et al (2013) Processing of emotional information in the human subthalamic nucleus. J Neurol Neurosurg Psychiatry 84(12):1331–1338. doi: 10.1136/jnnp-2011-302158.
7. Carpenter MB (1991) Core text of neuroanatomy (4th ed). Williams and Wilkins.
8. Chabardès S, Polosan M, Krack P et al (2012) Deep brain stimulation for obsessive-compulsive disorder: subthalamic nucleus target. World Neurosurg 80(3–4):S31.e1-8. doi: 10.1016/j.wneu.2012.03.010.
9. Chabardes S, Krack P, Piallat B et al (2020) Deep brain stimulation of the subthalamic nucleus in obsessive–compulsive disorders: Long-term follow-up of an open, prospective, observational cohort. JNNP 91(12):1349–1356. https://doi.org/10.1136/jnnp-2020-323421
10. Charbit AR, Akerman S, Holland PR, Goadsby PJ (2009) Neurons of the dopaminergic/calcitonin gene-related peptide A11 cell group modulate neuronal firing in the trigeminocervical complex: an electrophysiological and immunohistochemical study. J Neurosci 29(40):12532–12541. doi: 10.1523/JNEUROSCI.2887-09.2009.
11. Clemens S, Rye D, Hochman S (2006) Restless legs syndrome: revisiting the dopamine hypothesis from the spinal cord perspective. Neurology 67(1):125–130. doi: 10.1212/01.wnl.0000223316.53428.c9.
12. Coenen VA, Bewernick BH, Kayser S et al (2019) Superolateral medial forebrain bundle deep brain stimulation in major depression: a gateway trial. Neuropsychopharmacology 44(7):1224–1232. doi: 10. 1038/ s41386-019-0369-9.
13. Coenen VA, Schlaepfer TE, Goll P et al (2016) The medial forebrain bundle as a target for deep brain stimulation for obsessive-compulsive disorder. CNS Spectr 493:1–8. doi: 10. 1017/s1092 85291 60002 86.
14. Coenen VA, Schumacher LV, Kaller C et al (2018) The anatomy of the human medial forebrain bundle- Ventral tegmental area connections to reward-associated subcortical and frontal lobe regions. Neuroimage Clin 18:770–783. doi: 10. 1016/j.nicl. 2018. 03. 019.
15. Cossette M, Lévesque M, Parent A (1999) Extrastriatal dopaminergic innervation of human basal ganglia. Neurosci Res 34(1):51–54. doi: 10.1016/S0168-0102(99)00029-2.
16. Coudé D, Parent A, Parent M (2018) Single-axon tracing of the corticosubthalamic hyperdirect pathway in primates. Brain Struct Funct 223:3959–3973. doi: 10. 1007/ s00429-018-1726-x.
17. Dujardin K, Blairy S, Defebvre L, Krystkowiak P, Hess U, Blond S et al (2004) Subthalamic nucleus stimulation induces deficits in decoding emotional facial expressions in Parkinson's disease. J Neurol Neurosurg Psychiatry 75(2):202–208.

18. Dumas S, Wallén-Mackenzie Å (2019) Developmental Co-expression of Vglut2 and Nurr1 in a Mes-Di-Encephalic Continuum Preceeds Dopamine and Glutamate Neuron Specification. Front Cell Dev Biol 28;7:307. doi: 10.3389/fcell.2019.00307.
19. Eid L, Parent M (2015) Morphological evidence for dopamine interactions with pallidal neurons in primates. Front Neuroanat 9:111. doi: 10.3389/fnana.2015.00111.
20. Eid L, Parent A, Parent M (2014) Asynaptic feature and heterogeneous distribution of the cholinergic innervation of the globus pallidus in primates. Brain Struct Funct 221:1139–1155 (2016). doi: 10.1007/s00429-014-0960-0.
21. Eitan R, Shamir RR, Linetsky E et al (2013) Asymmetric right/left encoding of emotions in the human subthalamic nucleus. Front Syst Neurosci 7:69. doi: 10.3389/fnsys.2013.00069.
22. Fenoy AJ, Quevedo J, Soares JC (2021) Deep brain stimulation of the “medial forebrain bundle”: a strategy to modulate the reward system and manage treatment-resistant depression. Mol Psychiatry 27(1):574–592. doi: 10. 1038/ s41380-021-01100-6.
23. Ford B, Holmes CJ, Mainville L, Jones BE (1995) GABAergic neurons in the rat pontomesencephalic tegmentum: codistribution with cholinergic and other tegmental neurons projecting to the posterior lateral hypothalamus. J Comp Neurol 363(2):177–196. doi: 10.1002/cne.903630203.
24. Fortin-Houde J, Henserson F, Ducharme G, Amilhon B (2022) Parallel streams of raphe VGLUT3-positive inputs target the dorsal and ventral hippocampus in each hemisphere. bioRxiv 08.29.505760. doi: https://doi.org/10.1101/2022.08.29.505760
25. François C, Savy C, Jan C, Tande D, Hirsch EC, Yelnik J (2000) Dopaminergic innervation of the subthalamic nucleus in the normal state, in MPTP-treated monkeys, and in Parkinson’s disease patients. J Comp Neurol 425(1):121–129. doi: 10.1002/1096-9861(20000911)425:1<121::aid-cne10>3.0.co;2-g.
26. Franzini A, Broggi G, Cordella R et al (2013) Deep-brain stimulation for aggressive and disruptive behavior. World Neurosurg 80(3–4):S29.e11-4. doi: 10. 1016/j. wneu. 2012. 06. 038.
27. Franzini A, Ferroli P, Leone M, Broggi G (2003) Stimulation of the posterior hypothalamus for treatment of chronic intractable cluster headaches: First reported series. Neurosurgery 52(5):1095–1099; discussion 1099–1101.
28. Franzini A, Marras C, Ferroli P, Bugiani O, Broggi G (2005) Stimulation of the Posterior Hypothalamus for Medically Intractable Impulsive and Violent Behavior. Stereo Funct Neurosurg 83(2–3):63–66. doi: 10.1159/000086675
29. Fuxe K, Cintra A, Agnati LF, Härfstrand A, Goldstein M (1988) Studies on the relationship of tyrosine hydroxylase, dopamine and cyclic amp-regulated phosphoprotein-32 immunoreactive neuronal structures and d1 receptor antagonist binding sites in various brain regions of the male rat-mismatches indicate a role of d1 receptors in volume transmission. Neurochem Int 13(2):179–197. doi: 10.1016/0197-0186(88)90054-x.
30. Gippert SM, Switala C, Bewernick BH (2017) Deep brain stimulation for bipolar disorder-review and outlook. CNS Spectr 22(3):254–257. doi: 10.1017/S1092852915000577.

31. Hammond C, Yelnik J (1983) Intracellular labelling of rat subthalamic neurones with horseradish peroxidase: computer analysis of dendrites and characterization of axon arborization. Neuroscience 8(4):781–790. doi: 10.1016/0306-4522(83)90009-x.
32. Hardman CD, Henderson JM, Finkelstein DI (2002) Comparison of the basal ganglia in rats, marmosets, macaques, baboons, and humans: volume and neuronal number for the output, internal relay, and striatal modulating nuclei. J Comp Neurol 445(3):238–255. doi: 10.1002/cne.10165.
33. Haynes WIA, Haber SN (2013) The organization of prefrontal-subthalamic inputs in primates provides an anatomical substrate for both functional specificity and integration: implications for basal ganglia models and deep brain stimulation. J Neurosci 33:4804–4814. doi: 10. 1523/ jneur osci. 4674- 12. 2013.
34. Hedreen JC (1999) Tyrosine hydroxylase-immunoreactive elements in the human globus pallidus and subthalamic nucleus. J Comp Neurol 409(3):400–410. Doi: 10.1002/(sici)1096–9861(19990705)409:3 < 400:aid-cne5 > 3.0.co;2–<background-color:#D279AA;>4</background-color:#D279AA;>
35. Herbison AE, Horvath TL, Naftolin F, Leranth C (1995) Distribution of estrogen receptor-immunoreactive cells in monkey hypothalamus: relationship to neurones containing luteinizing hormone-releasing hormone and tyrosine hydroxylase. Neuroendocrinology 61(1):1–10. doi: 10.1159/000126810.
36. Johnson PL, Truitt W, Fitz SD et al (2010) A key role for orexin in panic anxiety. Nat Med 16(1):111–115. doi: 10.1038/nm.2075.
37. Johnson PL, Samuels BC, Fitz SD et al (2012) Activation of the orexin 1 receptor is a critical component of CO2-mediated anxiety and hypertension but not bradycardia. Neuropsychopharmacology 37(8):1911–1922. doi: 10.1038/npp.2012.38.
38. Karachi C, Yelnik J, Tandé D et al (2005) The pallidosubthalamic projection: An anatomical substrate for nonmotor functions of the subthalamic nucleus in primates. Mov Dis 20(2):172–180. doi: 10.1002/mds.20302
39. Kish SJ, Shannak K, Hornykiewicz O (1988) Uneven pattern of dopamine loss in the striatum of patients with idiopathic Parkinson's disease. Pathophysiologic and clinical implications. N Engl J Med 318(14):876–880. doi: 10.1056/NEJM198804073181402.
40. Kitahama K, Ikemoto K, Jouvet A (1998) Aromatic L-amino acid decarboxylase- and tyrosine hydroxylase-immunohistochemistry in the adult human hypothalamus. J Chem Neuroanat 16(1):43–55. doi: 10.1016/s0891-0618(98)00060-x.
41. Kruijver FP, Balesar R, Espila AM, Unmehopa UA, Swaab DF (2002) Estrogen receptor-alpha distribution in the human hypothalamus in relation to sex and endocrine status. J Comp Neurol 454(2):115–139. doi: 10.1002/cne.10416.
42. Kung L, Force M, Chute DJ, Roberts RC (1998) Immunocytochemical localization of tyrosine hydroxylase in the human striatum: a postmortem ultrastructural study. J Comp Neurol 390:52–62.

43. Lavoie B, Smith Y, Parent A (1989) Dopaminergic innervation of the basal ganglia in the squirrel monkey as revealed by tyrosine hydroxylase immunohistochemistry. J Comp Neurol 289(1):36–52. doi: 10.1002/cne.902890104.
44. Lee H, Kim DW, Remedios R, Anthony TE, Chang A, Madisen L et al (2014) Scalable control of mounting and attack by Esr1 + neurons in the ventromedial hypothalamus. Nature 509(7502):627–32. doi: 10.1038/nature13169.
45. Lévesque JC, Parent A (2005) GABAergic interneurons in human subthalamic nucleus. Mov Disord 20(5):574–84. doi: 10.1002/mds.20374.
46. Levitt P, Rakic P, Goldman-Rakic P (1984) Region-specific distribution of catecholamine afferents in primate cerebral cortex: a fluorescence histochemical analysis. J Comp Neurol 227(1):23–36. doi: 10.1002/cne.902270105.
47. Mai JK, Assheuer J, Paxinos G (1997) Atlas of the human brain. Academic Press.
48. Mallet L, Polosan M, Jaafari N et al (2008) Subthalamic nucleus stimulation in severe obsessive-compulsive disorder. N Engl J Med 359(20):2121–2134. doi: 10.1056/NEJMoa0708514.
49. Mallet L, Schüpbach M, N'Diaye K et al (2007) Stimulation of subterritories of the subthalamic nucleus reveals its role in the integration of the emotional and motor aspects of behavior. Proc Natl Acad Sci U S A 104(25):10661–10666. doi: 10.1073/pnas.0610849104.
50. Micieli R, Rios AL, Aguilar RP, Posada LF, Hutchison WD (2017) Single-unit analysis of the human posterior hypothalamus and red nucleus during deep brain stimulation for aggressivity. J Neurosurg 126(4):1158–1164. doi: 10.3171/2016.4.JNS141704.
51. Miguel Telega L, Ashouri Vajari D, Stieglitz T, Coenen VA, Döbrössy MD (2022) New Insights into In Vivo Dopamine Physiology and Neurostimulation: A Fiber Photometry Study Highlighting the Impact of Medial Forebrain Bundle Deep Brain Stimulation on the Nucleus Accumbens. Brain Sci 12(8):1105. doi: 10.3390/brainsci12081105.
52. Mori S, Takino T, Yamada H, Sano Y (1985) Immunohistochemical demonstration of serotonin nerve fibers in the subthalamic nucleus of the rat, cat and monkey. Neurosci Lett 62(3):305–309. doi: 10.1016/0304-3940(85)90566-x.
53. Nauta WJ, Haymaker W (1969) Hypothalamic nuclei and fiber connections. In: The hypothalamus, Thomas CC, editor. Springfi eld, Illinois, USA: Thomas Books. p. 136–200.
54. Nieuwenhuys R, Voogd J, van Huijzen C (2008) The human central nervous system. Springer, New York.
55. Ogawa S, Lubahn DB, Korach KS, Pfaff DW (1996) Behavioral effects of estrogen receptor gene disruption in male mice. Proc Natl Acad Sci USA 94(4):1476–1481. doi: 10.1073/pnas.94.4.1476.
56. Oldani L, Benatti B, Macellaro M et al (2021) A case of treatment-resistant bipolar depression and comorbid OCD treated with deep brain stimulation of the medial forebrain bundle: 5 years follow-up results. J Clin Neurosci 89:103–105. doi: 10.1016/j.jocn.2021.04.033.
57. Osterlund MK, Keller E, Hurd YL (2000) The human forebrain has discrete estrogen receptor alpha messenger RNA expression: high levels in the amygdaloid complex. Neuroscience 95(2):333–342.

doi: 10.1016/s0306-4522(99)00443-1.

58. Ourselin S, Roche A, Prima S, Ayache N (2000) Block Matching: A General Framework to Improve Improve Robustness of Rigid Registration of Medical Images. DiGioia A and Delp S (Eds), Third International Conference on Medical Robotics, Imaging And Computer Assisted Surgery (MICCAI 2000), Lectures Notes in Computer Science, pages 557–566, Pittsburgh, Penn, USA. Springer.
59. Parent M, Wallman MJ, Descarries L (2010) Distribution and ultrastructural features of the serotonin innervation in rat and squirrel monkey subthalamic nucleus. Eur J Neurosci 31(7):1233–1242. doi: 10.1111/j.1460-9568.2010.07143.x.
60. Perez S, Sendera TJ, Kordower JH, Mufson EJ (2004) Estrogen receptor alpha containing neurons in the monkey forebrain: lack of association with calcium binding proteins and choline acetyltransferase. Brain Res 1019(1–2):55–63. doi: 10.1016/j.brainres.2004.05.101.
61. Petrovich GD, Canteras NS, Swanson LW (2001) Combinatorial amygdalar inputs to hippocampal domains and hypothalamic behavior systems. Brain Res Brain Res Rev 38(1–2):247–289. doi: 10.1016/s0165-0173(01)00080-7.
62. Sakurai T (2007) The neural circuit of orexin (hypocretin): maintaining sleep and wakefulness. Nat Rev Neurosci 8(3):171–181. doi: 10.1038/nrn2092.
63. Sano K (1962) Sedative neurosurgery. Neurol Med-Chir 4:112–142. Doi: 10. 2176/ nmc.4. 112.
64. Sano K, Yoshioka M, Ogashiwa M et al (1966) Postero-medial hypothalamotomy in the treatment of aggressive behaviors. Stereot Funct Neurosci 27:164–167. doi: 10. 1159/ 00010 3949.
65. Sano K, Mayanagi Y, Sekino H et al (1970) Results of stimulation and destruction of the posterior hypothalamus in man. J Neurosurg 33:689–707. doi: 10. 3171/ jns. 1970. 33.6. 0689.
66. Schaltenbrand G, Wahren W, Hassler R (2005) Atlas for stereotaxy of the human brain: With an accompanying guide (2., revised and enlarged ed., 2. reprint). Thieme.
67. Schlaepfer TE, Bewernick BH, Kayser S, Mädler B, Coenen VA (2013) Rapid effects of deep brain stimulation for treatment-resistant major depression. Biol Psychiatry 73(12):1204–1212. doi: 10.1016/j.biopsych.2013.01.034.
68. Sébille SB, Rolland AS, Faillot M et al (2019) Normal and pathological neuronal distribution of the human mesencephalic locomotor region. Mov Disord 34(2):218–227.
69. Somma T, Esposito F, Scala MR et al (2022) Psychiatric Symptoms in Parkinson's Disease Patients before and One Year after Subthalamic Nucleus Deep Brain Stimulation Therapy: Role of Lead Positioning and Not of Total Electrical Energy Delivered. J Pers Med 3;12(10):1643. doi: 10.3390/jpm12101643. PMID: 36294782; PMCID: PMC9605574.
70. Soya S, Sakurai T (2018) Orexin as a modulator of fear-related behavior: Hypothalamic control of noradrenaline circuit. Brain Res 1731:146037. doi: 10.1016/j.brainres.2018.11.032.
71. Suzuki M, Beuckmann CT, Shikata K, Ogura H, Sawai T (2005) Orexin-A (hypocretin-1) is possibly involved in generation of anxiety-like behavior. Brain Res 1044(1):116–121. doi: 10.1016/j.brainres.2005.03.002.

72. Swaab DF (2003) Human Hypothalamus: Basic and Clinical Aspects, Part I. 1st Edition, Print Book.
73. Temiz G, Sébille SB, Francois C et al (2019) The anatomo-functional organization of the hyperdirect cortical pathway to the subthalamic area using in vivo structural connectivity imaging in humans. Brain Struct Funct 225:1–15. doi: 10. 1007/s00429-019-02012-6
74. Torres CV, Blasco G, García MN et al (2020) Deep brain stimulation for aggressiveness: long-term follow-up and tractography study of the stimulated brain areas. J Neurosurg 7:1–10. https://doi:10.3171/2019. 11. jns19 2608
75. Torres CV, Sola RG, Pastor J et al (2013) Long-term results of posteromedial hypothalamic deep brain stimulation for patients with resistant aggressiveness. J Neurosurg 119(2):277–287. doi: 10.3171/2013.4.JNS121639.
76. Veazey RB, Amaral DG, Cowan WM (1982) The morphology and connections of the posterior hypothalamus in the cynomolgus monkey (Macaca fascicularis). I. Cytoarchitectonic organization. J Comp Neurol 207(2):114–134. doi: 10.1002/cne.902070203.
77. Welter ML, Schüpbach M, Czernecki V et al (2014) Optimal target localization for subthalamic stimulation in patients with Parkinson disease. Neurology 82(15):1352–1361. doi: 10.1212/WNL.0000000000000315.
78. Yan H, Elkaim LM, Venetucci Gouveia F et al (2022) Deep brain stimulation for extreme behaviors associated with autism spectrum disorder converges on a common pathway: a systematic review and connectomic analysis. J Neurosurg 21:1–10. doi: 10.3171/2021.11.JNS21928.
79. Yelnik J, Bardinet E, Dormont D et al (2007) A three-dimensional, histological and deformable atlas of the human basal ganglia I. atlas construction based on immunohistochemical and MRI data. NeuroImage 34:618–638.
80. Zwirner J, Möbius D, Bechmann I et al (2017) Subthalamic nucleus volumes are highly consistent but decrease age-dependently-a combined magnetic resonance imaging and stereology approach in humans. Hum Brain Mapp 38(2):909–922. doi: 10.1002/hbm.23427.

Figures

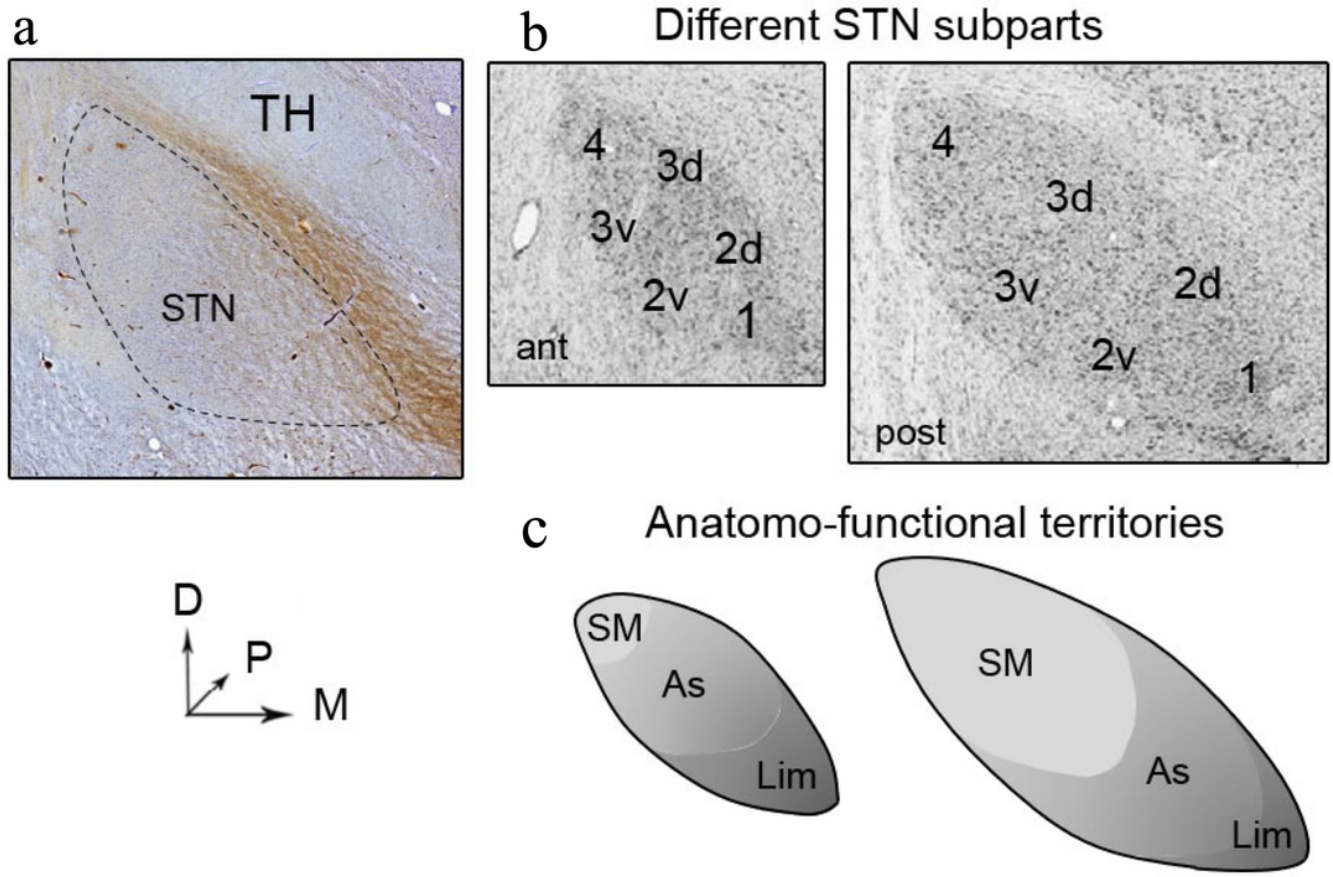

Figure 1

STN subparts (A) TH immunostained coronal section of the STN in human. (B) Light microscopic images of coronal STN sections counterstained with cresyl violet illustrating the subdivision of the STN into six subparts: n°1 for the anteromedial part, n°2 for the central part subdivided in a centrodorsal (n° 2d) and a centroventral (n° 2v) subparts, n°3 for the lateral part subdivided in a laterodorsal (n° 3d) and a lateroventral (n° 3v) subparts, and n°4 for the posterolateral part. (C) Schematic representation of the associative (As), sensorimotor (SM) and limbic (Lim) STN anatomo-functional territories based on external pallidal projections on two antero-posterior coronal sections of the STN in monkey. D, dorsal; Medial; P, posterior.

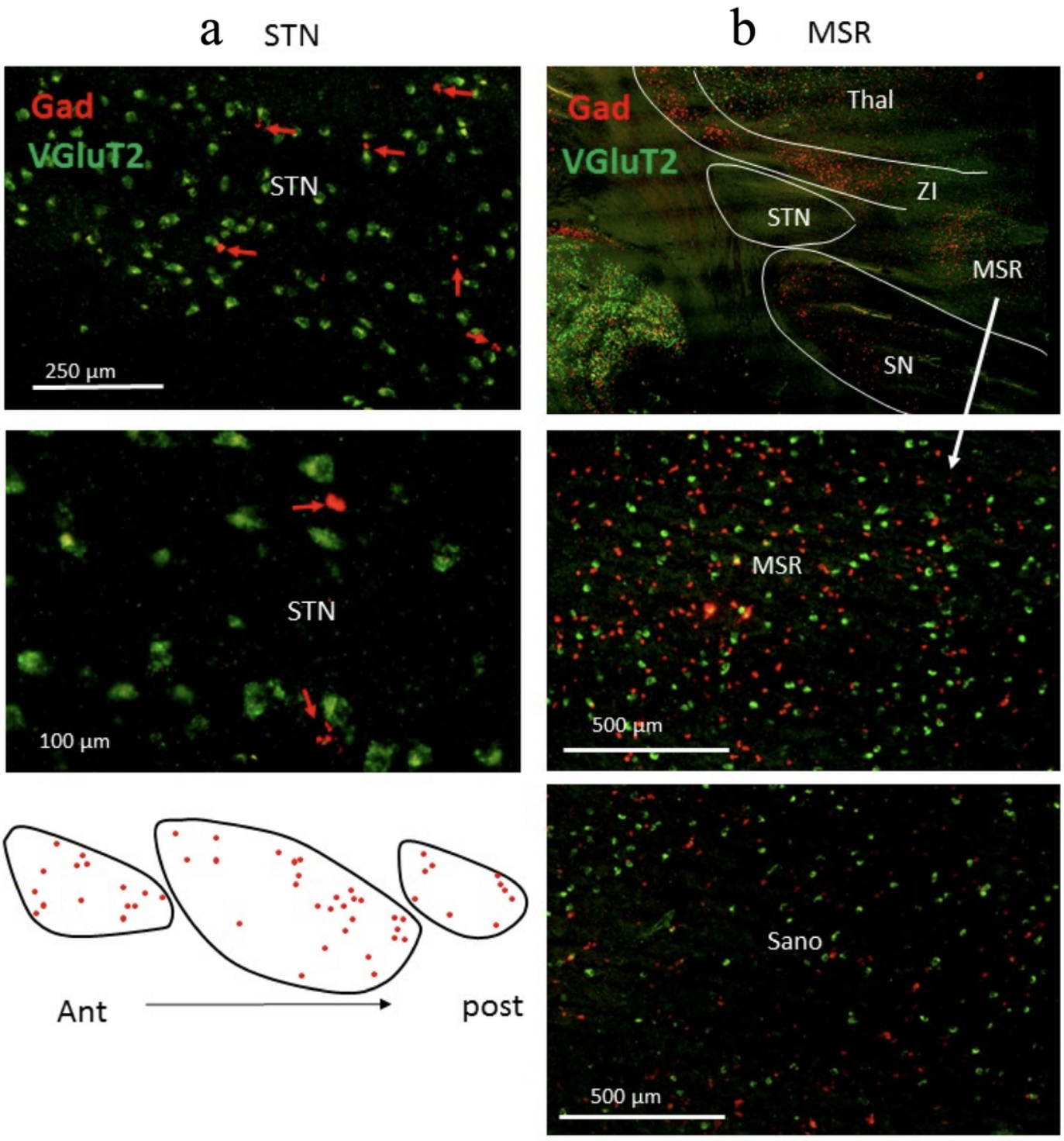

Figure 2

VGluT2 and Gad cell bodies in the monkey STN: (A) STN section showing the small population of neurons expressing Gad mRNA among neurons expressing VGluT2 mRNA stained using fluorescence *in situ*hybridisation. The cartography of these GABAergic neurons (red points) on three anteroposterior coronal sections shows their homogeneous distribution in the STN. (B) Sections double-stained for Gad and VGluT2 show that these neurons are present in both the MSR and the Sano triangle, but they are less

numerous in the later. Ant, anterior; MSR, medial subthalamic area; Post, posterior; Sano, triangle of Sano; SN, substantia nigra; Thal, thalamus; ZI, zona incerta.

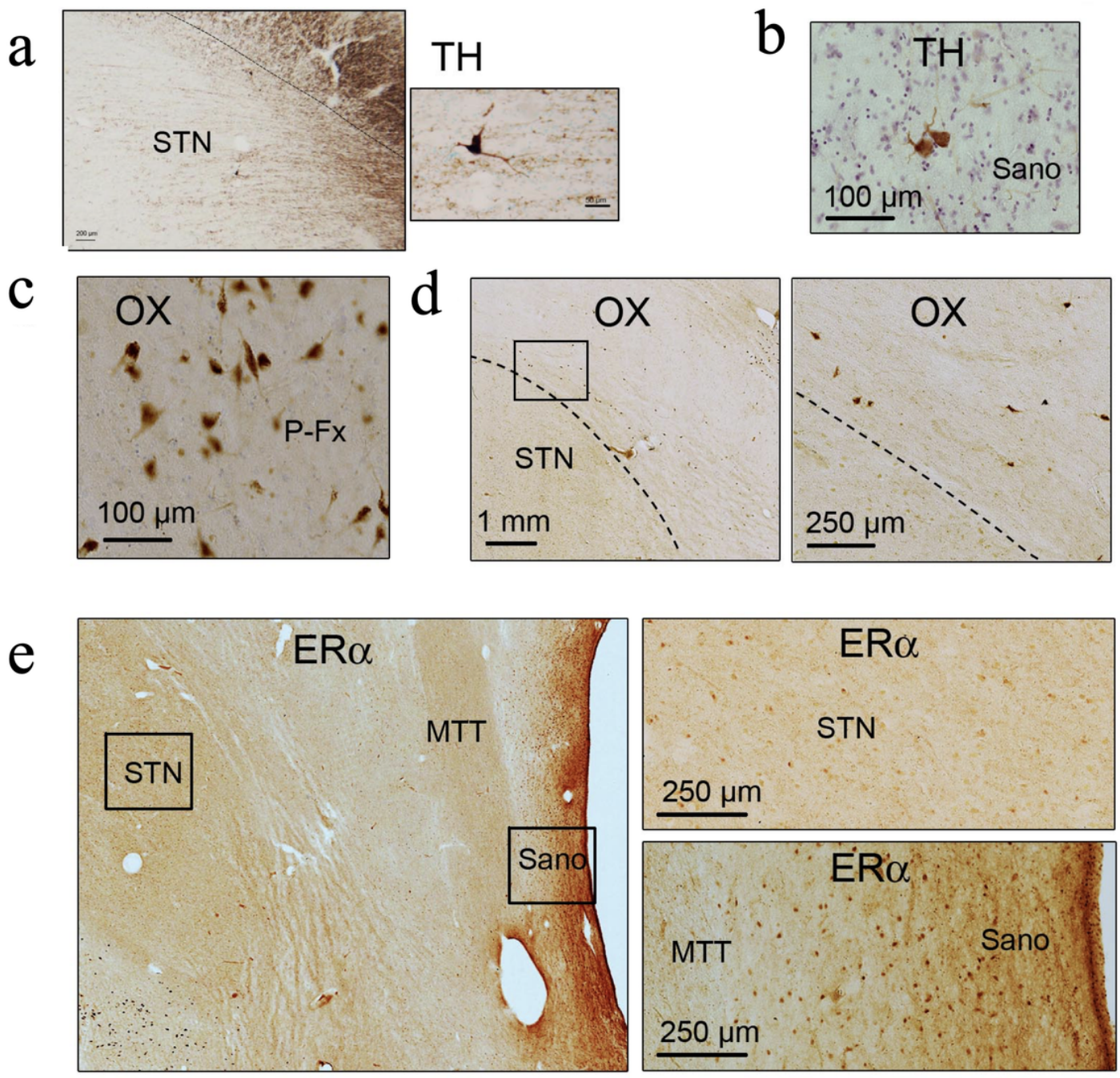

Figure 3

Various cell bodies in the MSR. (A) A TH+ cell body observed in the anterior and ventromedial part of the human STN at a low and high magnification. (B) 2 TH+ cell bodies observed in the Triangle of Sano. (C) OX+ cell bodies at the dorso-lateral border of the STN. The rectangle delineates the area shown at higher magnification at right. (D) Numerous OX+ cell bodies labelled in the peri-fornical area (P-Fx). (E) Cell bodies with strong oestrogen receptor (ERα) staining were dispersed over the whole MSR, with a

decreased mediolateral and anteroposterior gradient of density leading to dense staining anteromedially within the Sano triangle and to low staining in the medial STN subpart. MTT, mammillo-thalamic tract.

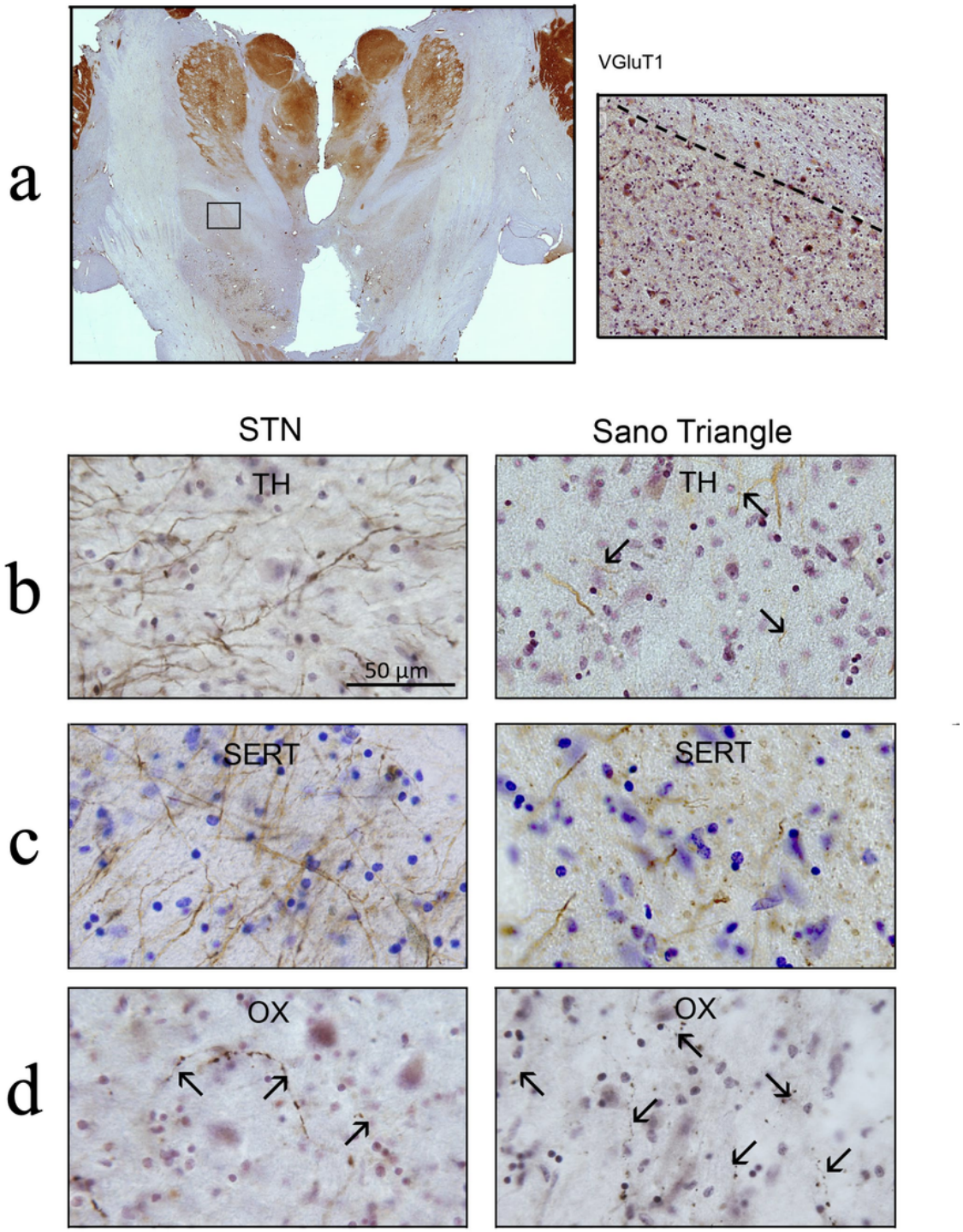

Figure 4

Various terminal axons in the MSR. (A) Low magnification photography showing that VGluT1 labelling appeared weaker in the STN compared to the strong labelling of the thalamus and striatum. VGluT1

labelling appears punctiform, as observed in the STN at high magnification. Examples of TH+ (B) SERT+ (C) and OX+ (D) axons seen in the medial STN (left), and in the Sano triangle (right)

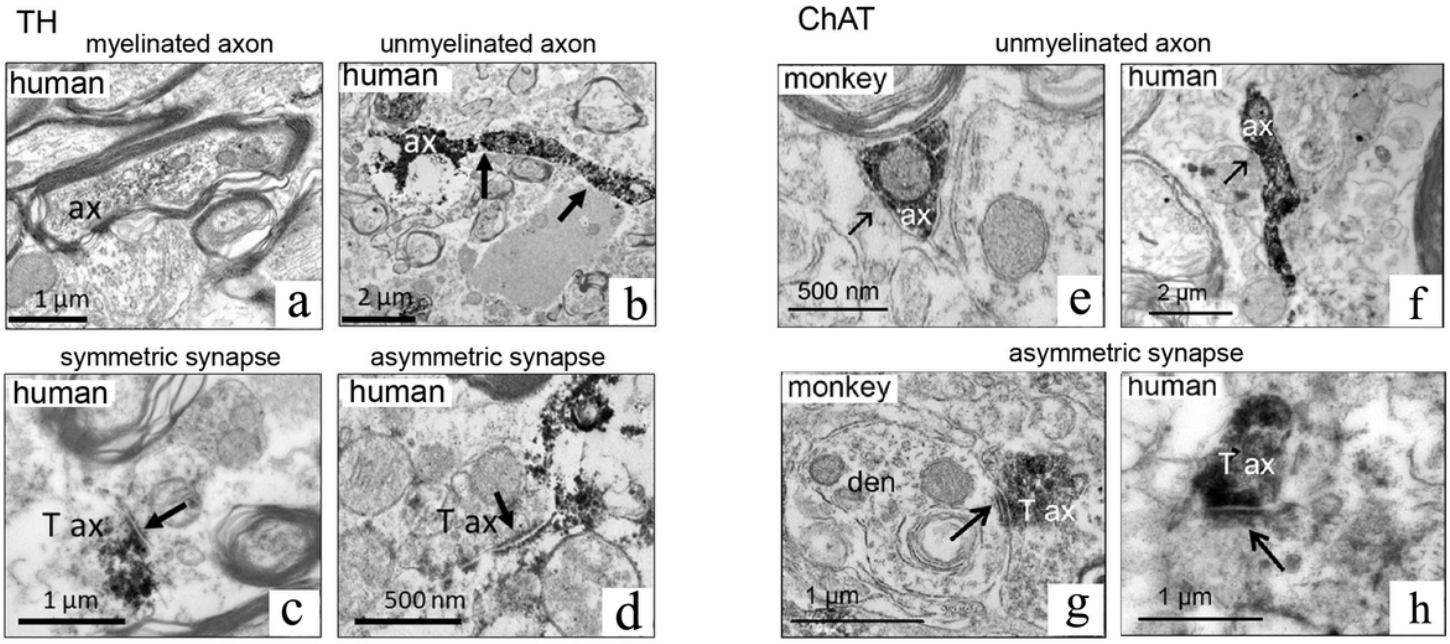

Figure 5

Electron microscopy of TH and ChAT immunostaining in the primate STN. Left: Examples of a myelinated axon (A), a long TH+ axon forming non-synaptic contacts (arrows) (B), and a terminal axon forming a symmetric (C) characterized by symmetric membrane specialisation, and an asymmetric synapse (arrows) (D) characterized by thick post-synaptic specialisation, in human. Right: Examples of small unmyelinated ChAT+ in monkey (E) and human (F), and a terminal axon forming asymmetric synapses in both species (G, H). Ax: axon; Den, dendrite; T ax, terminal axon.

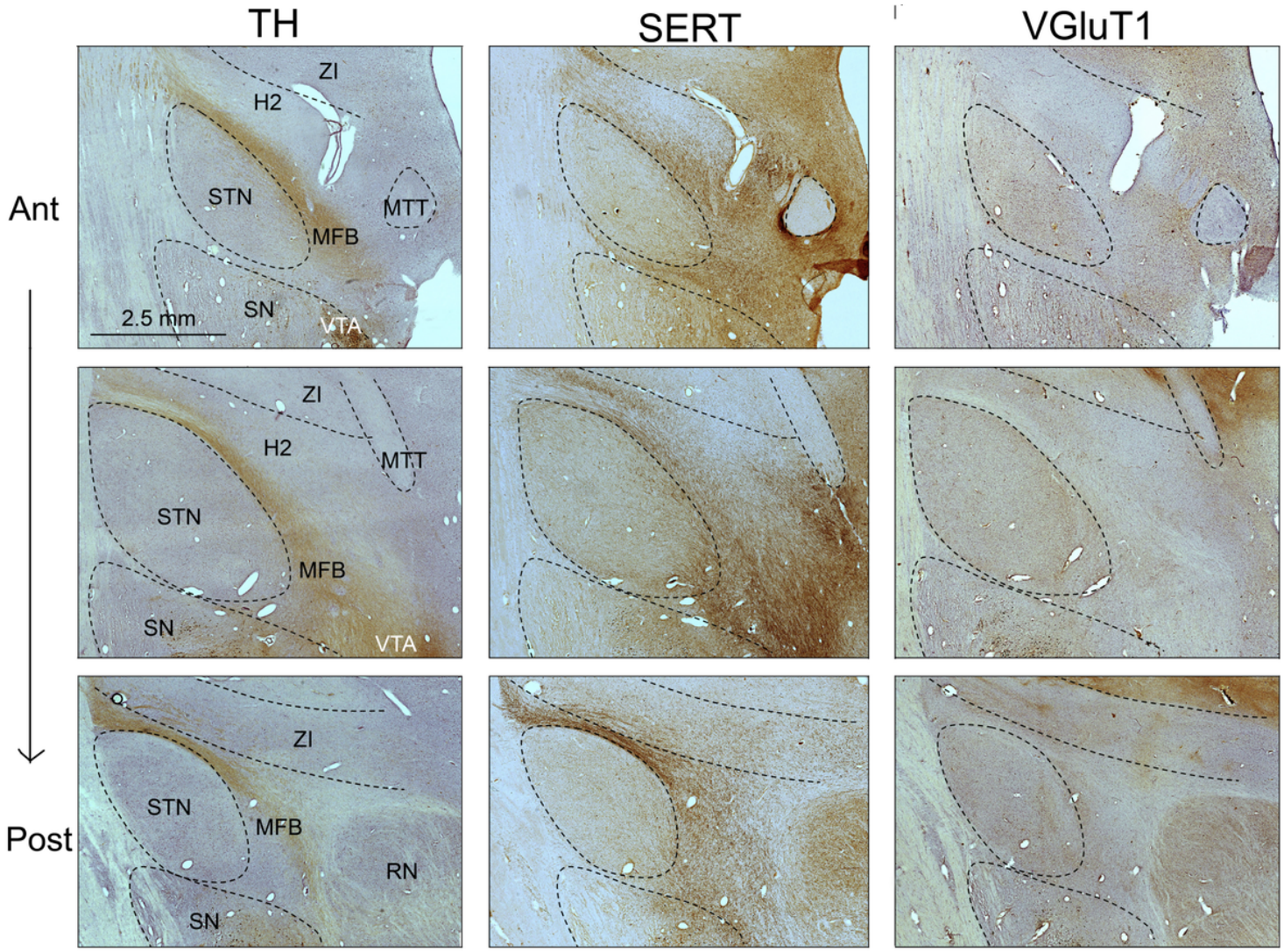

Figure 6

Various fibres in the MFB. Comparison of the distribution of TH (left), SERT (middle), and VGluT1 (right) immunostained axons on three adjacent sections from anterior (Ant) to posterior (Post) level of the MSR. Anteriorly, bundle of labelled TH fibres that mainly originate from the ventral tegmental area (VTA) and substantia nigra pars compacta (SN), together with a bundle of labelled SERT fibres course along the dorsal STN through the MFB. Posteriorly, at the level of the red nucleus (RN), numerous SERT+ fibres originating in the posterior raphe nucleus course postero-anteriorly and tend to be ventro-medially located relative to TH+ fibres. Comparatively, VGluT1+ fibres are more diffusely distributed in the MFB, and more generally within the whole extent of the MSR.

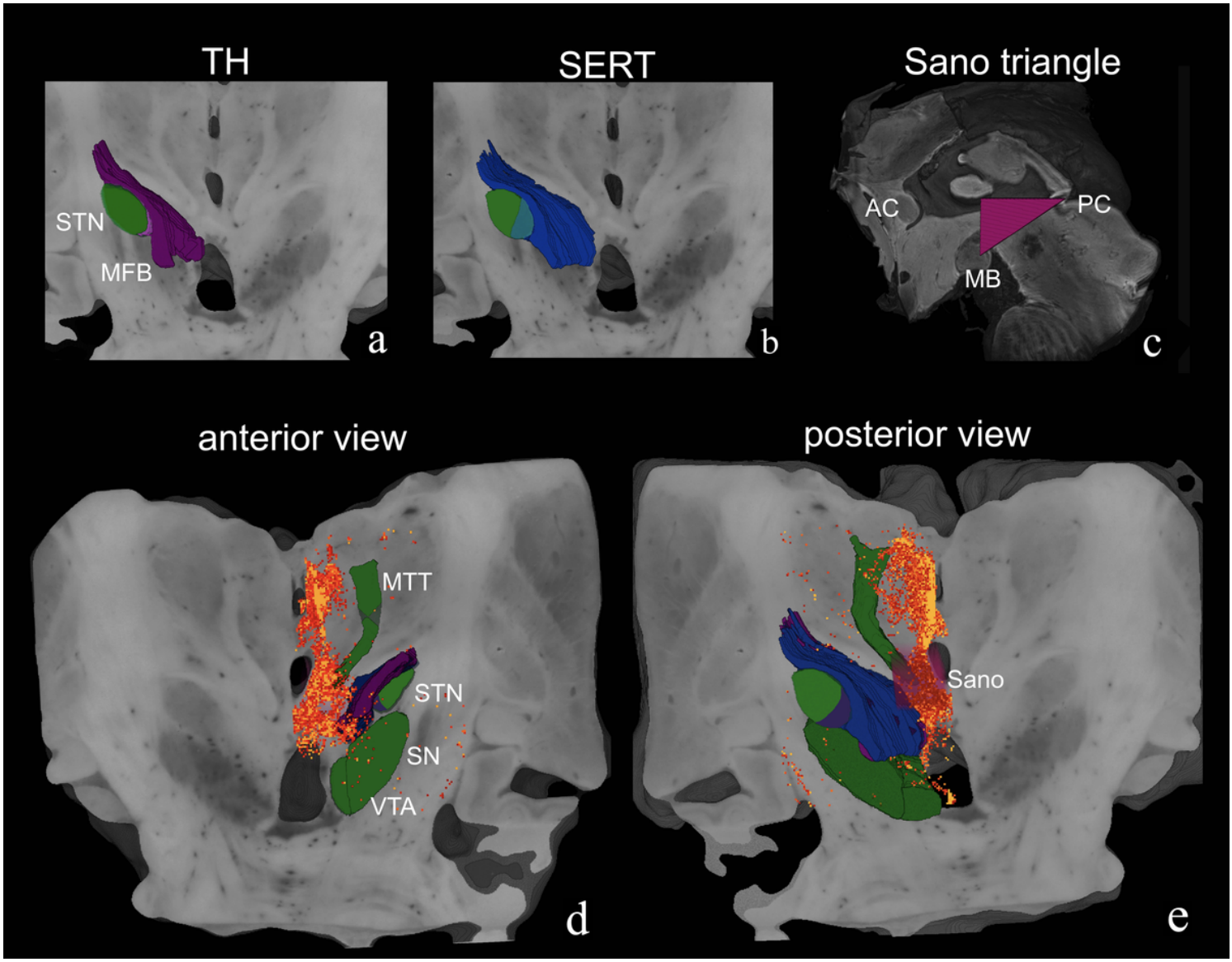

Figure 7

3D reconstruction illustrating the topographic relationships between the different major structures of the MSR. (A) Manual segmentation based on histological staining of TH-positive fibres and axon terminals (purple) and (B) SERT-positive fibres and axon terminals (blue) in the MFB and in the STN superimposed on a 3D coronal view of a representative coronal section of the cryobloc. (C) The triangle of Sano (pink) is delineated between the posterior commissure (PC), the mid commissural point, and the anterior mammillary body (MB) on a sagittal view of the T2* MRI. (D) Anterior (E) and posterior 3D view of manually segmented structures based on histological staining overlaid on a representative coronal section of the cryoblock. Mammillo-thalamic tract (MTT), substantia nigra (SN), subthalamic nucleus (STN), and ventral tegmental area (VTA) are represented in green, and the Sano triangle in pink. The difference in the density of neurons expressing Erα is represented in D and E, with brighter colours indicating higher neuron density.

Supplementary Files

This is a list of supplementary files associated with this preprint. Click to download.

- Supplementarydata.docx